Yinzhihuang oral liquid protects against non-alcoholic steatohepatitis via modulation of the gut-liver axis in mice

Shuyu Li[#]^, Fangyuan Chen[#]^, Yanting Zou^, Liuxin Ning^, Guangcong Zhang^, Shuncai Zhang^, Qunyan Yao^

Department of Gastroenterology and Hepatology, Zhongshan Hospital, Fudan University, Shanghai 200030, China; Shanghai Institute of Liver Diseases, Shanghai, China

Contributions: (I) Conception and design: All authors; (II) Administrative support: Q Yao, S Zhang; (III) Provision of study materials or patients: Q Yao, Y Zou, S Zhang; (IV) Collection and assembly of data: Q Yao, S Li, F Chen, Y Zou, L Ning, G Zhang; (V) Data analysis and interpretation: Q Yao, S Li, F Chen, Y Zou, G Zhang; (VI) Manuscript writing: All authors; (VII) Final approval of manuscript: All authors.

[#]These authors contributed equally to this work.

Correspondence to: Qunyan Yao; Shuncai Zhang. Department of Gastroenterology and Hepatology, Zhongshan Hospital, Fudan University, Shanghai 200030, China. Email: yao.qunyan@zs-hospital.sh.cn; zhang.shuncai@zs-hospital.sh.cn.

Background: Yinzhihuang (YZH) oral liquid is a traditional Chinese medicine compound that has emerged as a promising therapeutic agent for non-alcoholic fatty liver disease (NAFLD). Here, we aimed to investigate the therapeutic effects of YZH on non-alcoholic steatohepatitis (NASH) and elucidate its underlying molecular mechanisms.

Methods: Mice fed on a high-fat diet plus fructose/glucose drinking water (HFGD) were treated with YZH (30 mL/kg/d). The effects of YZH on mice with NASH were assessed through serological analysis and histological examination. Microbiota analysis based on 16S ribosomal ribonucleic acid (16S rRNA) and intestinal mucosal barrier function, serum inflammatory factors, hepatic macrophage infiltration, as well as hepatic toll-like receptor 4 (TLR4), myeloid differentiation primary response 88 (MyD88), nuclear factor kappa B (NFκB) pathway were carried out to explore the mechanism of YZH for treatment of NASH.

Results: Results of the current study found that YZH effectively reduced body weight gain and adiposity and alleviated hepatocyte steatosis, hepatocyte ballooning, liver tissue lobular inflammation, as well as fibrosis. It also reduced the accumulation of triglycerides, cholesterol, and free fatty acids in the liver of the treated mice and normalized serum aspartate transaminase, alanine transaminase, and glucose levels as well as lipid metabolism. Meanwhile, YZH treatment significantly decreased the abundance of harmful bacteria, such as *Mucispirillum*, *Helicobacter*, and *Desulfovibrionaceae*. Mechanistically, the present study found that YZH upregulated the expression of tight junction proteins, decreased serum lipopolysaccharide, interleukin 6, and tumor necrosis factor α levels, and increased interleukin 10 levels in serum. In the liver, YZH alleviated macrophage infiltration, especially that of pro-inflammatory macrophages. Moreover, it was found that YZH inhibited the canonical TLR4, MyD88, NFκB signaling pathway.

Conclusions: In conclusion, YZH may be a new agent for the prevention of NASH. Further, YZH alleviates gut microbiota dysbiosis, restores the intestinal mucosal barrier, and inhibits the canonical TLR4, MyD88, NFκB signaling pathway.

Keywords: Yinzhihuang oral liquid; non-alcoholic steatohepatitis (NASH); gut microbiota; gut-liver axis; nuclear factor kappa B (NFκB)

^ ORCID: Shuyu Li, 0000-0001-9318-5849; Fangyuan Chen, 0000-0002-0390-7957; Yanting Zou, 0000-0002-1470-4602; Liuxin Ning, 0000-0003-3548-0502; Guangcong Zhang, 0000-0003-3105-1903; Shuncai Zhang, 0000-0003-2031-4595; Qunyan Yao, 0000-0003-3586-1911.

Submitted Sep 12, 2021. Accepted for publication Mar 30, 2022.
doi: 10.21037/atm-21-4809
View this article at: https://dx.doi.org/10.21037/atm-21-4809

Introduction

In recent reports, metabolic-associated fatty liver disease (MAFLD) has been shown to fuel the development of chronic liver disease worldwide. Non-alcoholic steatohepatitis (NASH) is an aggressive subtype of MAFLD, characterized by hepatocyte injury (ballooning) and inflammation, accompanied with or without fibrosis (1). Patients with NASH have increased chances of developing cirrhosis, end-stage liver disease, or hepatocellular carcinoma as compared to patients with simple steatosis (2). Presently, data on the pathogenesis of NASH remains scant. Besides, there are no current Food and Drug Administration (FDA)-approved therapies for the treatment of NASH. Therefore, it is critical to evaluate the mechanisms underlying NASH pathogenesis to guide the development of effective drugs for the disease.

Although several previous studies have tried to define the mechanisms of NASH progression, the definitions remain controversial. The "multiple-hits hypothesis" is now widely used for explaining the pathogenesis of NASH (3). Such hits include alterations in lipid metabolism, oxidative stress, mitochondrial dysfunction, inflammation, insulin resistance, and endotoxins released by microbiota in the gut (4). In addition, the overgrowth of microbiota and disorders in the intestine microecology could perturb the functions of the intestinal barrier and increase gut permeability, leading to translocation of endotoxins and other inflammatory factors into the bloodstream (5,6). Furthermore, other studies have also indicated that the disruption of the gut barrier defines NASH pathogenesis (7). Therefore, imbalance of the intestinal microbiota mediates liver injury and disease progression from steatosis to steatohepatitis.

The use of Chinese herbs or their extracts has been shown to improve the prognosis of NASH in mice models (8-11). Yinzhihuang (YZH) oral liquid, a combination of several Chinese herbal medicines, was initially used in the treatment of neonatal jaundice and showed suppression of serum bilirubin concentration in newborns (12). Active ingredients in the YZH include *Artemisiae Scopariae Herba* (aerial parts of *Thunberg Artemisia scoparia* Waldst. et Kit. or *Artemisia capillaries* Thunb.), *Fructus Gardeniae* (fruits of *Gardenia jasminoides* Ellis), *Lonicierae Japonicae Flos* (flowers of *Lonicera japonica* Thunb.), and *Radix Scutellariae* (roots of *Scutellaria baicalensis* Georgi.) (13). Previous studies have shown that the YZH components can protect mice against the toxic effects associated with ectopic lipid deposition (14-18). It has also been demonstrated that the oral liquid can be effective in ameliorating diet-induced obesity and hepatic steatosis in our previous study (19). Notably, a recent report demonstrated that a combination of geniposide (extracted from *Fructus Gardeniae*) and chlorogenic acid (extracted from *Lonicerae Japonicae Flos*) ameliorated NASH in mice models (20). Therefore, these observations indicate that YZH may be useful in the treatment of NASH. However, the therapeutic effects and mechanisms of YZH against NASH are yet to be defined.

YZH is used for the treatment of neonatal jaundice by regulating metabolism of bile acid (12) and it has been found that the imbalance of bile acids is closely related to intestinal flora (21). In the present study, it was hypothesized that the effect of YZH on NASH might be through modulation of gut microbiota. Therefore, the present study examined the effects of YZH on the progression of NASH with a murine model established by a high-fat diet combined with fructose/glucose which simulates the human NASH metabolic profile. Mechanically the present study provided detailed insights on the role of YZH in the composition of gut microbiota, the intestinal barrier, serum inflammatory factors, liver macrophage phenotypes, hepatic toll-like receptor 4 (TLR4), myeloid differentiation primary response 88 (MyD88) and nuclear factor kappa B (NFκB) signal pathway. Results of the present study imply that YZH is a potential therapeutic agent that may be used for the treatment of NASH. Further, we present the following article in accordance with the ARRIVE reporting checklist (available at https://atm.amegroups.com/article/view/10.21037/atm-21-4809/rc).

Methods

Drug, animals and diets

A commercial product of YZH oral liquid was manufactured by China Resources Gaoke Natural Medicine Co. Ltd. (Beijing, China), following the Pharmacopoeia of People's Republic of China (PPRC) procedures (Commision, 2005). Briefly, its recipe is composed of 4 herbal medicine extracts:

12 g extract of *Artemisiae scopariae Herba* (aerial parts of *Thunberg Artemisia scoparia* Waldst. et Kit. or *Artemisia capillaries* Thunb.), 6.4 g extract of *Fructus gardeniae* (fruits of *Gardenia jasminoides* Ellis), 40 g extract of *Radix Scutellariae* (roots of *Scutellaria baicalensis* Georgi.), and 8 g extract of *Lonicierae Japonicae Flos* (flowers of *Lonicera japonica* Thunb.) for 1,000 mL liquid. Identification and quantification of marker compounded in YZH oral liquid were performed following the methods described in the PPRC. A voucher specimen (No. ZS-2021-1358) was deposited at the Department of Gastroenterology and Hepatology, Zhongshan Hospital, Fudan University. The C57BL/6J male mice aged 8 weeks old were purchased from Slack Laboratory Animal Co., Ltd. (Shanghai, China).

The mice were maintained in a temperature- and light-controlled environment and allowed free access to water and food. After 1 week of acclimatization, the mice were then randomly distributed into 3 groups with digital random method (n=6 per group, n=18 total groups): (I) mice were fed on a normal chow diet and normal drinking water (ND); (II) mice were fed on a high-fat diet purchased from Research Diets (cat. no. D12492; New Brunswick, NJ, USA) plus fructose/glucose purchased from Sigma-Aldrich (23.1 g l-fructose plus 18.9 g l-glucose in 1,000 mL autoclaved tap water after autoclaving, cat. no. F3510, G8270; St Louis, MO, USA) (HFGD) (22); and (III) mice were fed on a high-fat diet plus fructose/glucose and treated with YZH through gavage thrice per day at a dosage of 30 mL/kg/d (HFGD+Y) as previously described (19).

The weights of mice were monitored weekly. The mice were euthanized using pentobarbital sodium and blood samples were collected from inferior vena cava. Further, the liver, gut, and inguinal fat tissues were immediately collected, weighed, frozen in liquid nitrogen, and then stored at -80°C. All animals were used and cared according to the criteria of the Chinese Animal Protection Act and the National Research Council. Experiments were performed under a project license (No. 2018-67) granted by the Ethics Review Committee of Zhongshan Hospital Fudan University.

Measurement of blood and liver tissue

Blood was collected and centrifuged at 3,000 rpm for 10 min to separate the serum. Serum levels of triglycerides (TG), total cholesterol (TC), aspartate transaminase (AST), and alanine transaminase (ALT) were determined using the corresponding kits purchased from Nanjing Jiancheng Bioengineering Institute (Nanjing, China). Inflammatory factors were measured using ELISA kits which were purchased from ABclonal (Wuhan, China). Further, the level of lipopolysaccharide (LPS) was also measured using an ELISA kit purchased from CSB (Houston, TX, USA). FITC-dextran was used as a marker for gut mucosa permeability. The mice were gavaged with 0.6 mg/kg FITC-dextran obtained from Sigma-Aldrich 4 h before euthanasia. Serum FITC-Dextran levels were measured according to the manufacturer's instructions. 10 mg liver tissue was homogenized in a specific solvent and the levels of TG, cholesterol and free fatty acids (FFAs) in the resultant samples were measured using a Colorimetric/Fluorometric Assay Kit obtained from BioVision (San Francisco, CA, USA). All experimental procedures in the present study were performed according to instructions provided by the manufacturers.

Glucose metabolism

Tail vein blood was collected for fasting blood glucose test after a 16-week intervention period. The levels of fasting blood insulin were measured using a mouse insulin ELISA kit purchased from Millipore (Billerica, MA, USA). Insulin resistance was calculated using the standard formula as described in the previous studies (23). The intraperitoneal glucose tolerance test (IPGTT) and insulin tolerance test (ITT) were also performed to estimate glucose metabolism in mice. For the IPGTT and ITT, the mice were fasted for 12 and 4 h respectively at the 17th week of modeling and then intraperitoneally injected glucose (2.5 g/kg) for IPGTT or insulin (2.7 U/kg) for ITT. The tail vein blood was then collected and tested with a portable blood glucose meter purchased from Roche Group (Basel, Switzerland) to determine the glucose level immediately before the intraperitoneal injection and subsequently at 15-, 30-, 60-, 90-, and 120-min post-administration. Feeding was resumed immediately after the experiment.

Hydroxyproline test

Hydroxyproline levels (as an index of collagen) in liver tissue were measured in duplicate using colorimetric methods, according to the hydroxyproline test kit instructions purchased from the Institute of Jiancheng Bioengineering (Nanjing, China). Briefly, 50 of liver tissue was hydrolyzed with 1ml hydrolysate, water bath at 95 ℃, for 20 min. After cooling the test tube to room temperature in flowing water, 10 μL of PH indicator, solution A and solution B were

successively added to each tube to adjust PH to 6.0–6.8. Then the solution in the test tube was diluted to 10 mL. An appropriate quantity of activated carbon was added into 4 mL of diluted hydrolysate and the mixture was centrifuged at 3,500 rpm for 10 min to get supernatants. We used 100 μL of supernatants to determine the hydroxyproline content with the hydroxyproline standard at 550 nm wavelength. The collagen level was calculated from the product of the hydroxyproline content (micrograms per milligram of protein, mg/mg prot) according to the formulae given in the instructions.

RNA isolation and real-time polymerase chain reaction

Total ribonucleic acid (RNA) was isolated from the tissues using a column RNA extraction kit obtained from Promega (Madison, WI, USA) and was reverse transcribed to complementary deoxyribonucleic acid (cDNA) using GoScript™ Reverse Transcription Mix, Random Primers purchased from Promega. To quantify the transcripts of the genes of interest, the present study used SYBR Green Premix obtained from Promega on an ABI Prism 7500 Sequence Detection System purchased from Applied Biosystems (Foster City, CA, USA). Relative target gene expression was analyzed using the $2^{-\Delta\Delta Ct}$ method, with β-actin as a control. The appropriate primers for polymerase chain reaction (PCR) are listed in the Table S1. The experimental procedures described earlier were performed according to the instructions provided by the manufacturer. The current study selected the amplified cDNA, synthesized into double-stranded DNA, modified, connected, and amplified using specific primers. The products were then heat-denatured into a single strand using a bridge primer for cyclization and charge-qualification before sequencing. After alignment with reference sequences, the level of gene expression was determined and the differentially expressed genes were then analyzed.

Western blot analysis

Proteins were isolated from the liver and gut tissue using radio-immunoprecipitation assay (RIPA) buffer purchased from Beyotime Biology (Shanghai, China) containing a protease and phosphatase inhibitor cocktail purchased from Beyotime Biology. After pulverization using a bead mill homogenizer purchased from Jingxin (Shanghai, China), the protein was quantified using a bicinchoninic acid (BCA) kit purchased from Beyotime Biology. Consequently, 40 mg of protein was separated on a polyacrylamide gel and transferred onto a polyvinylidene difluoride membrane purchased from Millipore. After incubation with 5% bovine serum albumin (BSA) purchased from Service Biology (Wuhan, China) blocking for 1 h, membranes were incubated overnight, with the primary antibody in a 4 ℃ refrigerator. The secondary antibody was incubated for 1 h then, and the bands were detected using a chemiluminescent horseradish peroxidase (HRP) substrate purchased from Millipore. Densitometric band analysis was performed using a Gel-Pro Analyzer 4 from Media Cybernetics Corporation (Rockville, MD, USA).

16S rRNA amplicon sequencing

Genomic DNA was isolated from mouse focal samples using the QIAamp Fast DNA Stool Mini Kit purchased from Qiagen (Dusseldorf, Germany), following the instructions provided by the manufacturer. The V4 region of the 16S ribosomal RNA (rRNA) gene was amplified using the forward primer 341F (5'-CCTACGGGAGGCACAG-3') attached to the Roche B adapter for Illumina library construction and the reverse primer 806R (5'-GGACTACNVGGGTWTCTAAT-3') attached to the Roche A adapter and a 10-nt barcode [5'-A-adapter-N (10) +16S primer-3'].

The DNA libraries were sequenced using the Illumina MiSeq platform, following the instructions provided by manufacturer. Then 16S Ribosomal RNA Gene Amplicons were prepared for the Illumina MiSeq 2500 System. Subsequently, FLASH v1.2.7 software was used to merge the reads and then Trimmomatic v0.33 was used to filter and clean the Tags. After removing chimeras using UCHIME v4.2, the paired-end joined sequences were grouped into operational taxonomic units for subsequent analysis.

Histopathological examinations

After normal saline perfusion, the liver, gut, and inguinal fat tissues were fixed in 4% polyoxymethylene purchased from Servicebio (Wuhan, China) for 24 h. The samples were then dehydrated and embedded in paraffin. Finally, the embedded tissue was cut into 5-μm-thick sections and stained by hematoxylin and eosin (H&E), Oil red O, Sirius red, and immunohistochemistry (IHC) (19,24). The terminal ileum tissue was fixed, dehydrated, sectioned at 60 nm, applied to copper grids, and imaged using transmission electron microscopy from HITACHI (Tokyo, Japan).

Immunohistochemistry and quantitative analysis of histological markers

Liver sections treated as described earlier were deparaffinized, hydrated, and incubated with 3% hydrogen peroxide. Heat-induced antigen retrieval was performed in a target retrieval solution, following the protocol provided by the manufacturer. The primary antibodies anti-F4/80 and anti-interferon regulatory factor 5 (IRF-5) purchased from Cell Signaling Technology Inc. (Danvers, MA, USA) were applied to the sections at 4 ℃ overnight. Then the sections were subsequently washed and incubated with HRP-conjugated goat anti-rabbit or anti-mouse IgG secondary antibodies purchased from Jackson Immunoresearch Inc. (Cambridge, UK) for 1 hour at 37 ℃ in an incubator. 3,3'-diaminobenzidine tetrachloride purchased from Beyotime Biology was used as a chromogen substrate and hematoxylin was used to counterstain the slides.

Immunoreaction visualization and a negative control setup were performed according to the same procedure. Images were taken under a high-power field with a BX43 microscope purchased from Olympus (Tokyo, Japan).

Statistical analysis

All data were expressed as mean ± standard deviation (SD). Statistical analysis was performed with GraphPad Prism software (version 8.0; La Jolla, CA, USA). The analysis of variance (ANOVA) was used to compare between groups after normal distribution test. If normality or homogeneity of variance was not met, Kruskal-Walli's test was used to compare between groups. A value of $P<0.05$ was considered to be statistically significant.

Results

YZH reduced the body, liver, and fat weight of mice fed HFGD

To investigate the protective effects of YZH on NASH *in vivo*, a high-fat diet plus fructose/glucose-induced murine NASH model was established which could present more profound inflammation and fibrosis in the liver than the HFD-induced model. It was found that the bodyweight of mice fed HFGD increased at a noticeably faster pace than that of mice fed ND, whereas the rate of weight gain of mice fed HFGD + Y lied between the mice fed HFGD and ND (*Figure 1A,1B*), regardless of that they had similar food intake (*Figure 1C*).

Meanwhile, it was observed that the mice in HFGD + Y group had no diarrhea. Further, it was found that there were no significant differences in the 24-h stool weight and the number of pellets among the 3 groups of mice (Figure S1). The increasing trend of liver and inguinal fat weight was concordant with the trend of weight gain. After 17 weeks of HFGD feeding, the results of the present study found that the liver size and weight were larger than those of the mice fed ND.

In addition, it was observed that the livers extracted from HFGD-fed mice were visibly yellow and greasy with blunt edges. However, the administration of YZH significantly decreased the liver weight of mice fed on HFGD, enabling liver appearance similar to that of ND-fed mice (*Figure 1D,1E*). Meanwhile, it was found that the gavage of YZH markedly reduced the weight and volume of inguinal fat in HFGD-fed mice (*Figure 1D-1F*).

YZH decreased SAF score and the volume of inguinal fat cells in NASH mice

Similar to the trend of weight gain as described earlier, HFGD-fed mice demonstrated severely aggregated hepatic steatosis, inflammation, and fibrosis as compared with ND-fed mice. The liver sections of HFGD-fed mice exhibited a large area of macrovesicular steatosis around the central vein (68.9% of the total area) and were accompanied by lobular inflammation in H&E staining (*Figure 2A,2B*).

Results of the present study showed that large lipid droplets mixed with small lipid droplets stained in red were observed in the liver sections of HFGD-fed mice in Oil-red staining (*Figure 2A-2C*). Further, several collagen fiber depositions were visualized in the peri-vein hepatic sinusoids of HFGD-fed mice in Sirius red staining (*Figure 2A*). On the contrary, the liver sections of HFGD + Y-fed mice showed a smaller area of lipid droplets, as well as inflammation, and revealed no collagen fiber deposition (*Figure 2A-2C*).

Similar to histological examination, hydroxyproline content in the liver was significantly increased in HFGD-fed mice as compared with ND-fed mice, whereas HFGD + Y-fed mice had significantly lower hydroxyproline content as compared with HFGD-fed mice (*Figure 2D*). In addition to the liver, the H&E staining of the inguinal sections also indicated more giant fat cells in HFGD-fed mice than in ND-fed mice, whereas the inguinal fat cells of HFGD + Y-fed mice were significantly smaller than those of HFGD-fed mice (*Figure 2A,2E*). Overall, it was evident that all the histopathological results showed that YZH decreased the

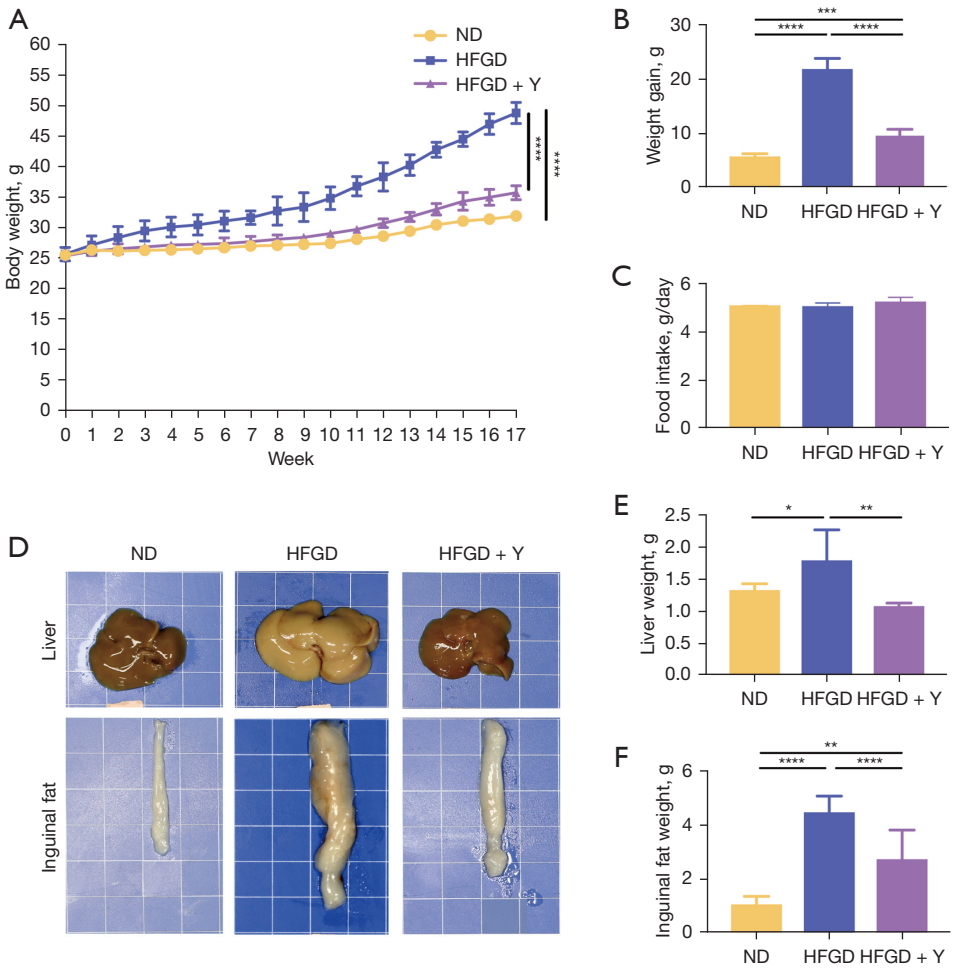

Figure 1 Yinzhihuang (YZH) reduced body weight, liver weight, and fat weight of mice fed with high-fat diet plus fructose/glucose drinking water (HFGD). C57/BL6J mice were divided into 3 groups: the control group was given normal food and drinking water and was given an equal volume of normal saline by gavage (ND group); the model group was given high-fat food and high-sugar water and was given an equal volume of normal saline by gavage (HFGD group); the treatment group was given high-fat food and high-sugar water and 30 mL/kg/d YZH by gavage (HFGD + Y group). (A) Changes in body weight of mice in each group with feeding time; (B) weight gain of mice in each group compared with initial body weight; (C) daily food intake of mice in each group; (D) representative gross image of liver and inguinal fat of mice in each group; (E) comparison of the liver weight of mice; (F) comparison of the inguinal fat weight of mice. N=6. Data were expressed as mean ± SD. *P<0.05, **P<0.01, ***P<0.001, ****P<0.0001.

steatosis activity fibrosis (SAF) score in the NASH mouse model (*Figure 2F*).

YZH reduced liver lipid accumulation and serum aminotransferase levels in NASH mice

To further investigate the effect of YZH on steatosis and inflammation in NASH mice, the levels of triglycerides, cholesterol, FFA, and transaminases were measured in the current study. It was found that the accumulation of triglycerides in liver was significantly increased in HFGD group, which was 4 times that of ND group (*Figure 3A*). In addition, both cholesterol and FFAs in HFGD group were also increased by 1.3 times as compared with that in ND group (*Figure 3B,3C*). However, the levels of triglycerides, cholesterol, and FFA of mice in HFGD + Y group were significantly lower than those in HFGD group (*Figure 3A-3C*). This suggested that YZH could significantly reduce liver triglycerides, cholesterol, and FFA deposition. Further, the levels of ALT and AST in the blood were

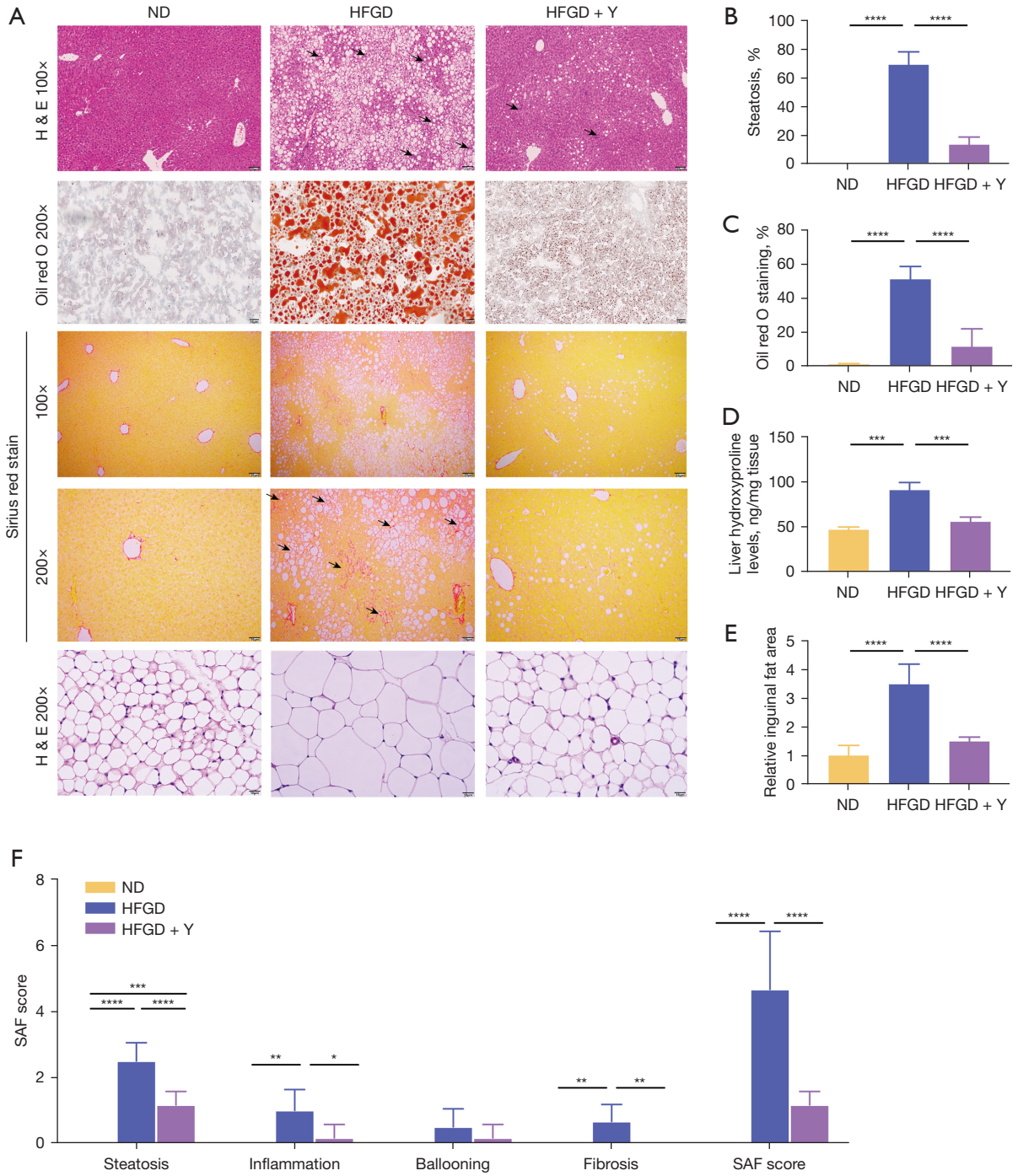

Figure 2 Yinzhihuang (YZH) decreased steatosis activity fibrosis (SAF) score and the volume of inguinal fat cells in non-alcoholic steatohepatitis (NASH) mice. (A) The representative photograph of hematoxylin and eosin (H&E) staining, Oil red O and Sirius red staining of liver paraffin section, together with H&E staining of inguinal adipose tissue paraffin section; the arrows in the liver H&E staining indicated the lobular inflammation area, and the arrows in the Sirius red staining indicated the collagen deposition area. (B) The evaluation of liver steatosis based on H&E staining; (C) the evaluation of liver steatosis based on Oil red O; (D) hydroxyproline content in the liver tissues of the 3 groups of mice; (E) the evaluation of the relative inguinal fat area based on H&E staining; (F) SAF score of each group. Data were expressed as mean ± SD. *P<0.05, **P<0.01, ***P<0.001, ****P<0.0001.

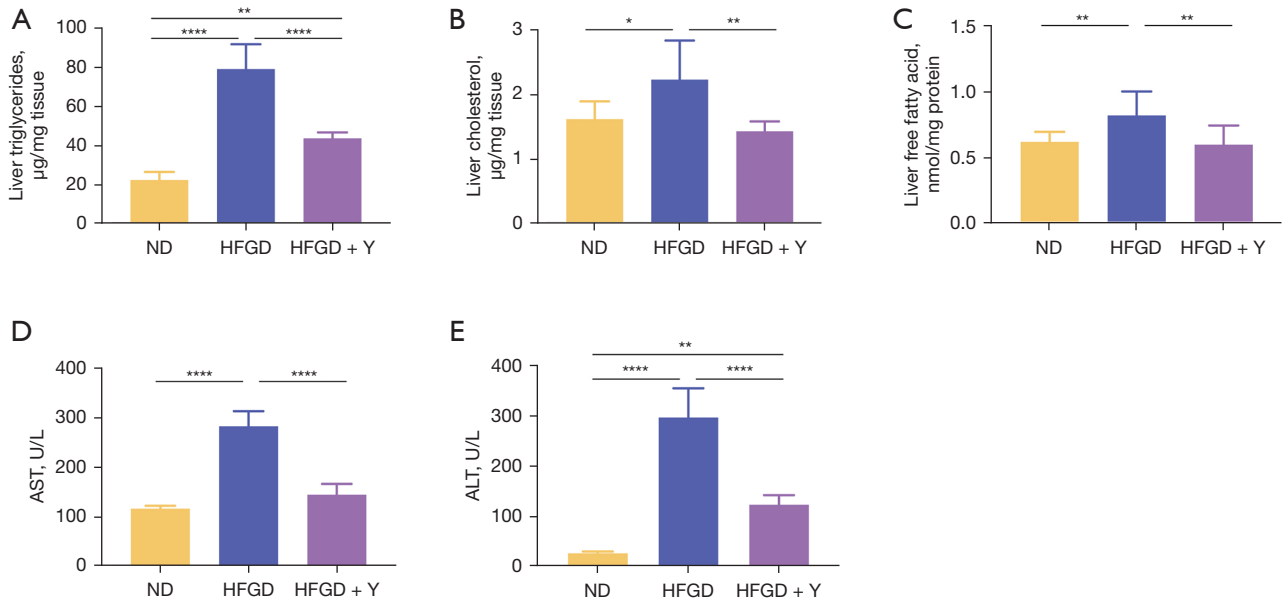

Figure 3 Yinzhihuang (YZH) reduced liver lipid accumulation and serum aminotransferase levels in non-alcoholic steatohepatitis (NASH) mice. (A) Liver triglycerides content in each group; (B) liver cholesterol content in each group; (C) liver free fatty acid content in each group; (D) serum aspartate aminotransferase level of 3 groups of mice; (E) serum alanine aminotransferase level of 3 groups of mice. Data were expressed as mean ± SD. *P<0.05, **P<0.01, ****P<0.0001.

examined to determine the severity of hepatocyte damage. Results of this study showed that the levels of ALT and AST were significantly higher in HFGD group than in ND group, but lower in HFGD + Y group as compared with HFGD group (*Figure 3D,3E*).

YZH improved glucolipid metabolic disorders in NASH mice

Since disorders of glucolipid metabolism are typical characteristics of NASH, indicators of glucose and lipid metabolism were also detected in the present study. The level of serum triglycerides in HFGD group increased substantially compared to that in ND group. Similarly, the level of serum total cholesterol of HFGD-fed mice also increased to a certain extent (*Figure 4A,4B*). In comparison, it was evident that YZH decreased the levels of both serum triglycerides and total cholesterol in HFGD-fed mice (*Figure 4A,4B*).

As for glucose metabolism, the fasting blood glucose in HFGD group was significantly increased as compared with that in ND group. However, the fasting blood glucose was reduced in HFGD + Y group as compared to HFGD group, but it was still higher than that in ND group (*Figure 4C*). Further, the fasting blood insulin level and insulin resistance index in HFGD group were higher than those in ND group, and YZH noticeably decreased the fasting blood insulin level and insulin resistance index in NASH mice (*Figure 4D,4E*). Furthermore, results of the IPGTT experiment indicated that the ability of mice in HFGD group to regulate blood glucose was significantly weakened whereas treatment with YZH restored the ability (*Figure 4F*). Meanwhile, results of the ITT experiment showed that blood glucose levels in HFGD group were constantly at a high level within 90 min after the injection of insulin. However, the level of blood glucose in HFGD + Y group had a significant initial decrease after the insulin injection, followed by an increase over time, which was in line with the trend observed in ND group (*Figure 4G*).

YZH regulated the composition of intestinal flora

The 16S rRNA sequencing was performed on the feces of 3 groups with 6 samples in each group and performed a series of species diversity analyzes to investigate the effect of YZH on species diversity of intestinal flora. First, the degree of similarity between 3 sets of samples in terms of species diversity was assessed. Results of both the principal component analysis and coordinate analysis of the present

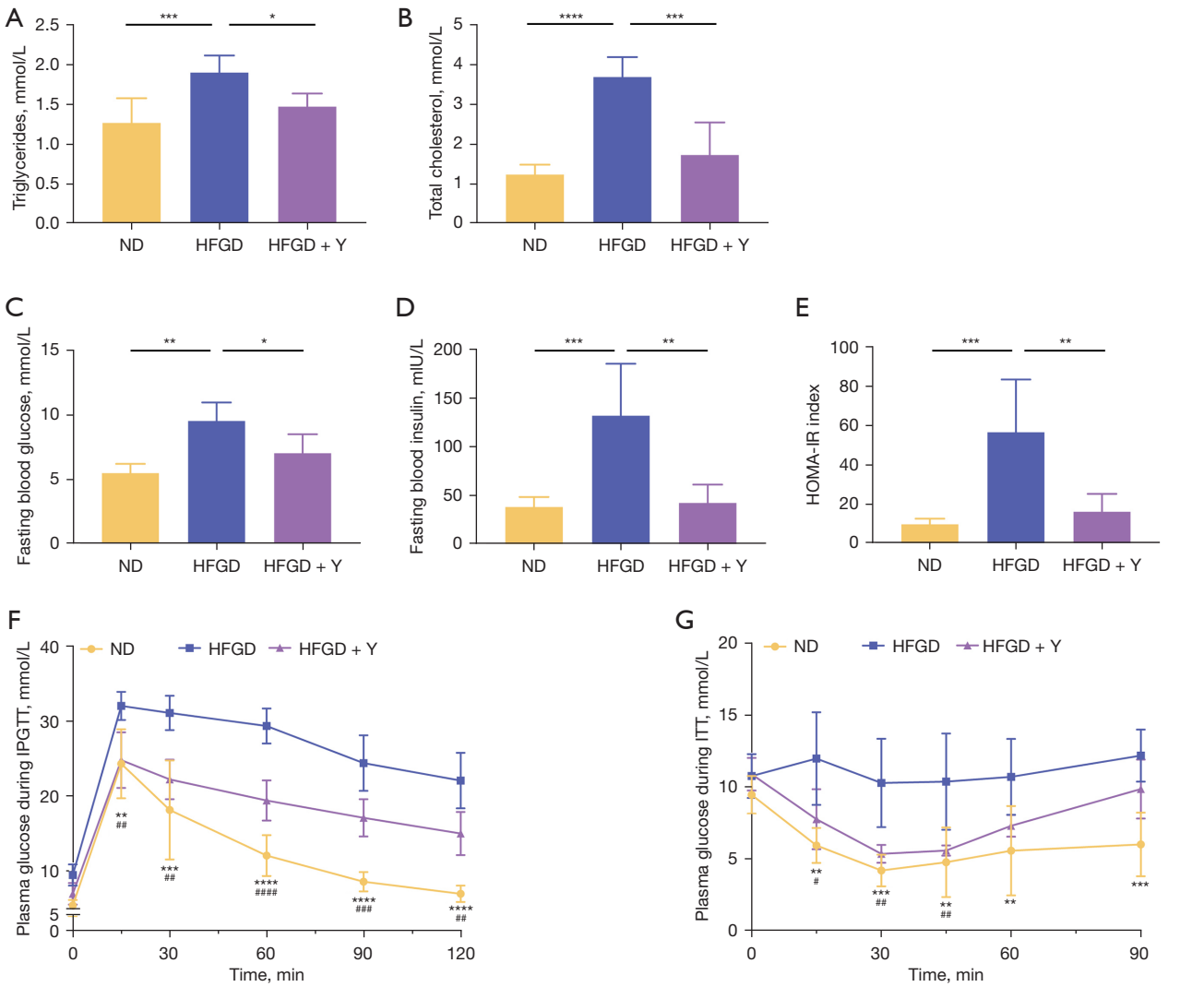

Figure 4 Yinzhihuang (YZH) improved glucolipid metabolic disorders in non-alcoholic steatohepatitis (NASH) mice. (A) Serum triglyceride content in each group; (B) serum total cholesterol content in each group; (C) fasting blood glucose levels in each group; (D) fasting blood insulin levels in each group; (E) insulin resistance index in each group; (F) intraperitoneal glucose tolerance test in 3 groups of mice; (G) insulin tolerance test in 3 groups of mice. Data were shown as mean ± SD. ND *vs.* high-fat diet plus fructose/glucose drinking water (HFGD), *P<0.05, **P<0.01, ***P<0.001, ****P<0.0001; HFGD *vs.* HFGD + Y, $^{\#}$P<0.05, $^{\#\#}$P<0.01, $^{\#\#\#}$P<0.001, $^{\#\#\#\#}$P<0.0001.

study indicated that species composition of the intestinal flora of mice in HFGD group was markedly different from that of the other 2 groups, whereas the species composition of the intestinal flora of HFGD + Y group was more similar to that of ND group (*Figure 5A*,*5B*).

The differences in the intestinal flora of the 3 groups of mice at the phylum and genus levels were also investigated. The gut community of mice in the 3 groups was composed of 10 bacterial phyla, including *Firmicutes*, *Bacteroidetes*, *Proteobacteria*, *Verrucomicrobia*, *Actinobacteria*, *Tenericutes*, *Cyanobacteria*, *Patescibacteria*, *Epsilonbacteraeota*, and *Deferribacteres*, except for other undefined and low-content bacteria (*Figure 5C*). Among them, *Firmicutes* and *Bacteroides* were the main phyla and the ratio of *Firmicutes/Bacteroides* in the feces of mice in HFGD group was significantly higher than that in ND group. Interestingly, YZH could reduce the ratio of *Firmicutes/Bacteroides* (*Figure 5D*). Furthermore, the top 10 bacterial genera were listed as follows: *Muribaculaceae*, *Lachnospiraceae*, *Desulfovibrionaceae*, *NK4A136* (*Lachnospiraceae*_NK4A136_group), *Helicobacter*,

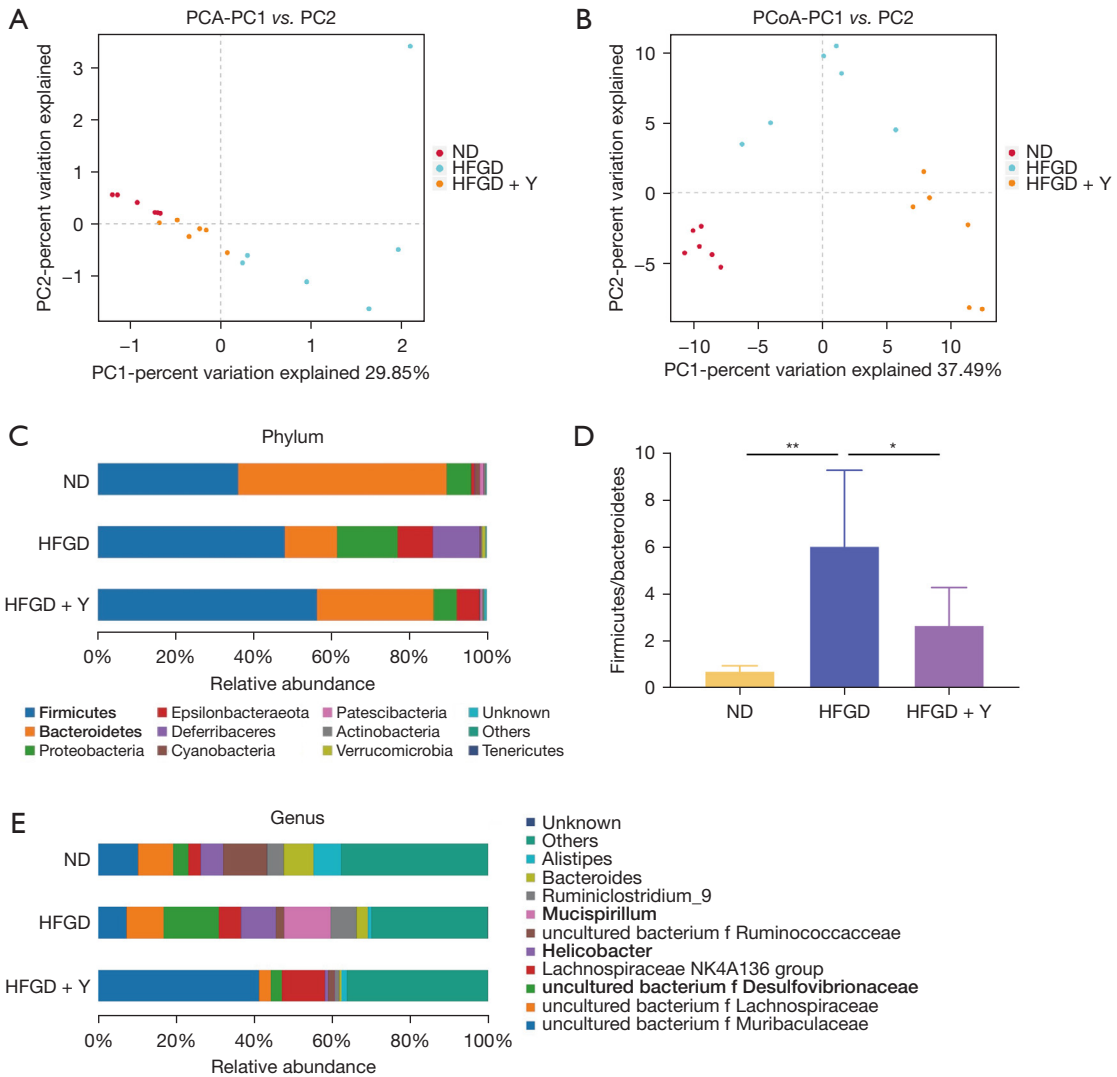

Figure 5 YZH regulated the composition of intestinal flora. (A) Principal component analysis (PCA) of the 3 groups; (B) principal coordinate analysis (PCoA) of the 3 groups; (C) differences in the phylum level of the intestinal flora of the 3 groups of mice; (D) differences in the ratio of Firmicutes/Bacteroidetes in the 3 groups of mice; (E) differences in the genus level of the intestinal flora of the 3 groups of mice. Data were shown as mean ± SD. *P<0.05; **P<0.01. YZH, yinzhihuang.

Ruminococcaceae, *Mucispirillum*, *Ruminoclostridium_9*, *Bacteroides*, *and Alistipes* (*Figure 5E*). The abundance of *Muribaculaceae* in HFGD group was significantly reduced as compared with ND group, whereas the abundance of *Desulfovibrionaceae*, *Helicobacter*, *Ruminoclostridium_9*, and *Mucispirillum* was significantly increased as compared with ND group (*Figure 5E*). Correspondingly, the abundance of *Muribaculaceae* in HFGD + Y group was significantly higher than that in HFGD group, while the abundances of *Desulfovibrionaceae*, *Helicobacter*, *Ruminoclostridium_9,* and *Mucispirillum* were lower (*Figure 5E*).

YZH protected the intestinal mucosal barrier and reduced endotoxemia

LPS is the major component of the outer membrane of gram-negative bacteria. Since YZH could regulate the species diversity of intestinal flora, the present study further examined LPS levels in each group. Results showed that the level of LPS was higher in HFGD group than that in ND group and HFGD-Y group (*Figure 6A*). It was noted that the level of intestinal *Desulfovibrionaceae* was found to correlate positively with levels of LPS in the blood (*Figure 6B*).

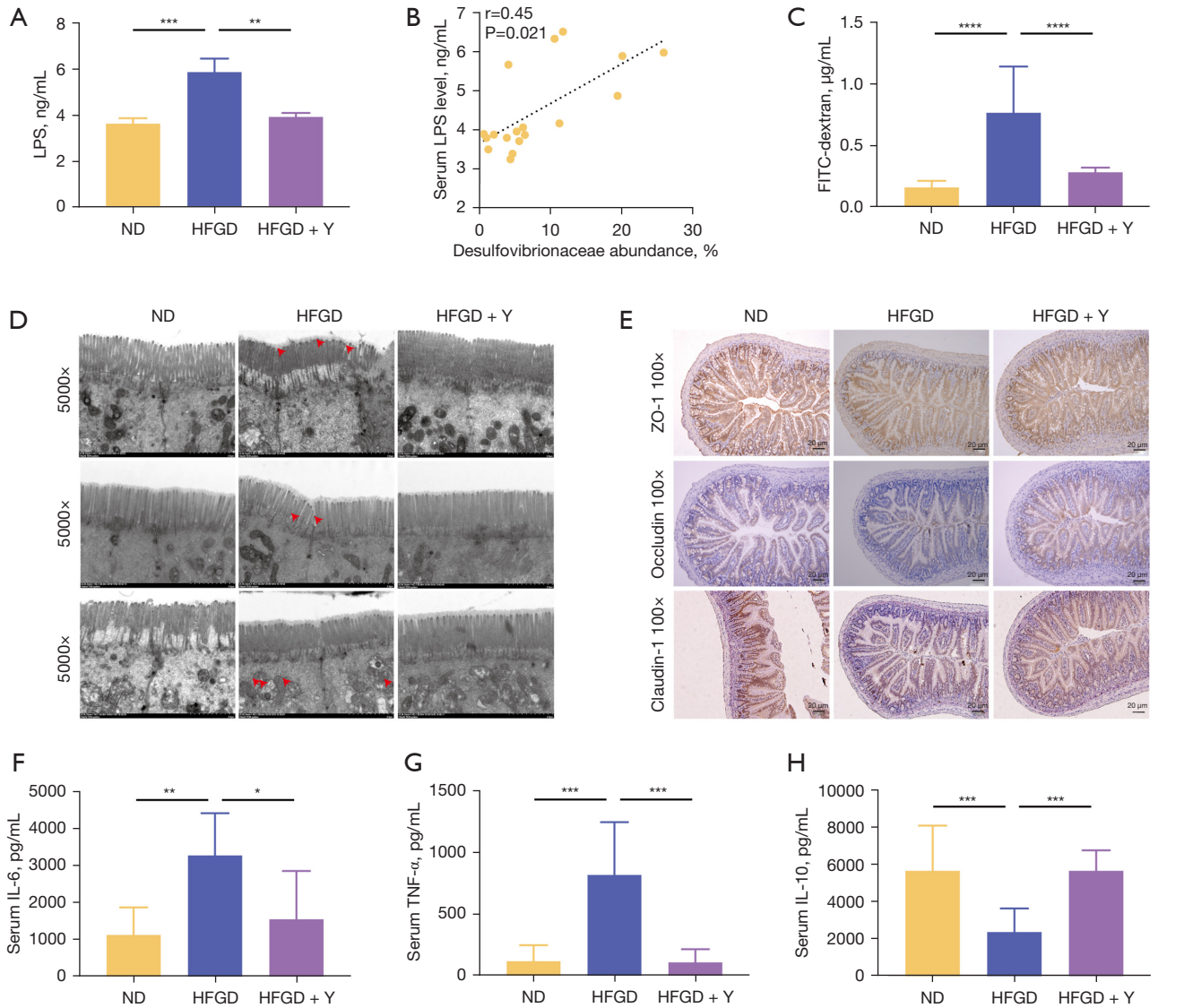

Figure 6 YZH protected the intestinal mucosal barrier and reduced endotoxemia. (A) Serum LPS levels in the 3 groups of mice; (B) Spearman correlation analysis between Desulfovibrio and blood LPS; (C) Serum FITC-Dextran levels in the 3 groups of mice; (D) representative electron micrographs of the terminal ileum of the 3 groups of mice. The upper images indicated the degree of edema of the intestinal microvilli; the middle images indicated the shortness of the intestinal microvilli; the lower images indicated the decrease of the mitochondrial cristae. Red arrows indicated typical parts. (E) The protein levels of ZO-1, occludin, and claudin-1 were evaluated by immunohistochemistry; (F) serum IL-6 levels in each group; (G) serum TNF-α levels in each group; (H) serum IL-10 levels in each group. Data were shown as mean ± SD. *P<0.05; **P<0.01; ***P<0.001; ****P<0.0001. YZH, yinzhihuang; LPS, lipopolysaccharide; ZO-1, zonula occludens 1; IL-6, interleukin-6; TNF-α, tumor necrosis factor alpha; IL-10, interleukin-10 .

The permeability of the intestinal mucosa at the end of the ileum was significantly increased in HFGD group as changes in serum FITC-dextran levels indicated in this study, whereas YZH significantly reduced the permeability of the intestinal mucosa on a high-fat and -sugar diet mouse model (*Figure 6C*). Electron microscopy revealed that microvilli of the terminal ileum mucosa became shortened, edema, and the disappearance of mitochondria in HFGD group as compared with ND group. On the other hand, it was found that the microvilli of the terminal ileum mucosa in HFGD + Y group showed no obvious structural abnormalities (*Figure 6D*). Meanwhile, zonula occludens 1

(ZO-1), occludin, and claudin-1 were presented with the highest expressions in the terminal ileum of ND mice, whereas their expressions in HFGD+Y mice were higher than those in HFGD mice (*Figure 6E*).

Accompanied by dysregulated intestinal permeability, the levels of pro-inflammatory cytokines, including interleukin-6 (IL-6) and tumor necrosis factor alpha (TNF-α), in HFGD group were significantly higher than those in ND group and HFGD + Y group, whereas no significant difference was observed in the latter 2 groups (*Figure 6F,6G*). On the contrary, the level of anti-inflammatory factor, interleukin-10 (IL-10), significantly decreased in HFGD group as compared with ND group and HFGD + Y group, with no significant difference in the latter 2 groups (*Figure 6H*).

YZH decreased pro-inflammatory macrophages and relieved liver inflammation

The number of total macrophages and pro-inflammatory macrophages in the liver was assessed as shown in *Figure* 7 to further clarify the effect of YZH on liver inflammation. The infiltration of liver macrophages (F4/80+) was significantly increased and promoted in HFGD group as compared with ND group and the number of pro-inflammatory macrophages (IRF5+) was consistently elevated. Meanwhile, the infiltration of macrophages and the number of pro-inflammatory macrophages were notably reduced in HFGD + Y group as compared with HFGD group (*Figure 7A-7D*). In addition, the results of the present study showed that the inflammatory factors in liver, including monocyte chemoattractant protein 1 (MCP-1) and interleukin-1 beta (IL-1β), were also markedly decreased in HFGD + Y group as compared with HFGD group (*Figure 7E,7F*).

YZH attenuated NASH by inhibiting the TLR4, MyD88, NFκB pathway

To investigate the mechanism by which YZH alleviates liver inflammation, the levels of related proteins in the canonical TLR4, MyD88, NFκB pathway in the liver tissues of 3 groups of mice, including TLR4, MyD88, inhibitor of NFκB alpha (IκBα), p-IκBα, NFκB and p-NFκB were detected in the current study. Results of the current study showed that the protein levels of TLR4, MyD88, p-IκBα, and p-NFκB in HFGD group were significantly higher than those in ND group (*Figure 8A,8B*), whereas those in HFGD + Y group were observably lower than in HFGD group. These findings suggest that YZH can significantly protect against and alleviate NASH by inhibiting the TLR-4, MyD88, NFκB pathway.

Discussion

Recently, there has been increasing interest in the treatment of patients with NASH using natural plant products due to their long-term therapeutic efficacy and low toxicity (25-28). The findings of our previous study showed that YZH ameliorated obesity and lipid metabolism disorders, reduced serum AST, as well as ALT levels, and degenerated hepatic steatosis in high-fat diet mice (19). The current study showed that YZH ameliorated high fat and glucose diet-induced liver injury via altering the composition of the gut microbiota in mice, which restored the function of the intestinal barrier and reduced the levels of circulating LPS and pro-inflammatory factors. Therefore, this data provide new insights into the mechanisms underlying the therapeutic effects of YZH against NASH.

The YZH oral liquid, a traditional Chinese medicine compound, has emerged as a promising therapeutic agent in the treatment of NAFLD (19,29). Over the past decades, YZH has been shown to treat neonatal jaundice, with a good safety profile and efficacy (12). However, data on the mechanisms of actions are yet to be defined. High-fat and -glucose diets have been deemed to be most consistent with the dietary habits of patients with metabolic syndrome and are broadly applied in NASH-related research (30-32). This model covers several pathophysiological features of human NASH, such as insulin resistance, lipid accumulation, hepatocyte ballooning, inflammatory cell infiltration, and perisinusoidal fibrosis (33). Moreover, multiple mechanisms have been proposed for HFGD model (34-36).

The active ingredients in YZH including geniposide, scoparone, baicalein, and chlorogenic acid have been shown to confer anti-inflammatory and antioxidative activities (37-41). Notably, it has been reported that these major components, separately or in combination, can be used to treat NAFLD *in vivo* and/or *in vitro* models (14,16,20,39,42). Therefore, the current study used YZH as a formulation instead of the active ingredients since its monomer cannot retain the comprehensive effects brought about by drug interactions, and YZH has good safety in clinical medication. In a high-fat diet mouse model, it was found that YZH reduced body weight and the degree of hepatic steatosis (19). In the present study, a 16-week high-fat and -glucose/fructose diet led to severe liver steatosis, mild inflammation,

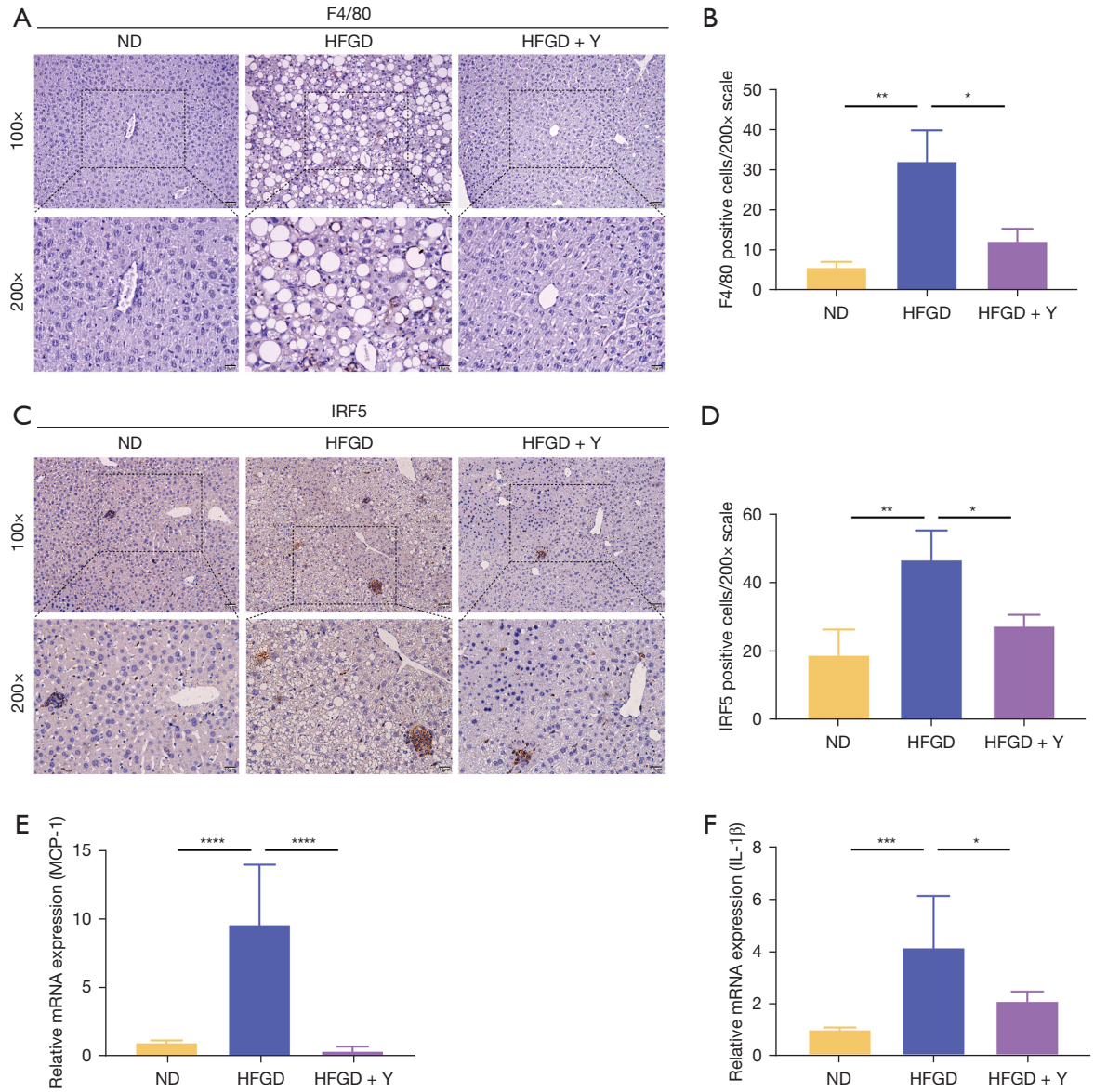

Figure 7 YZH decreased pro-inflammatory macrophages and relieved liver inflammation. (A) The expression of F4/80 in liver was evaluated by immunohistochemistry; (B) the statistics of F4/80 positive cells in each group; (C) the expression of IRF5 in liver was evaluated by IHC; (D) the statistics of IRF5 positive cells in each group; (E) the expression of monocyte MCP-1 at the mRNA level of the 3 groups of mice; (F) the expression of IL-1β at the mRNA level of the 3 groups of mice. Data were shown as mean ± SD. *P<0.05; **P<0.01; ***P<0.001; ****P<0.0001. YZH, yinzhihuang; IRF5, interferon regulatory factor 5; IHC, immunohistochemistry; MCP-1, chemoattractant protein 1; mRNA, ribosomal ribonucleic acid; IL-1β, interleukin-1 beta.

and mild fibrosis. It was also shown that YZH remarkably decreased the degree of steatosis, inflammation, and fibrosis. Results of the present study also showed that YZH alleviated hepatic injury, as evidenced by decreased AST and ALT levels. Further, it was evident that YZH played a key role in regulating glucose metabolism. In addition, it was demonstrated that intrahepatic triglycerides, cholesterol, and free fatty acids levels decreased after YZH treatment.

The gut microbiota interacts with the host in many different organs, such as the liver, brain, and kidney (21,43,44). The gut-liver axis indicates the interactions between the gut and liver, hence the gut microbiota plays

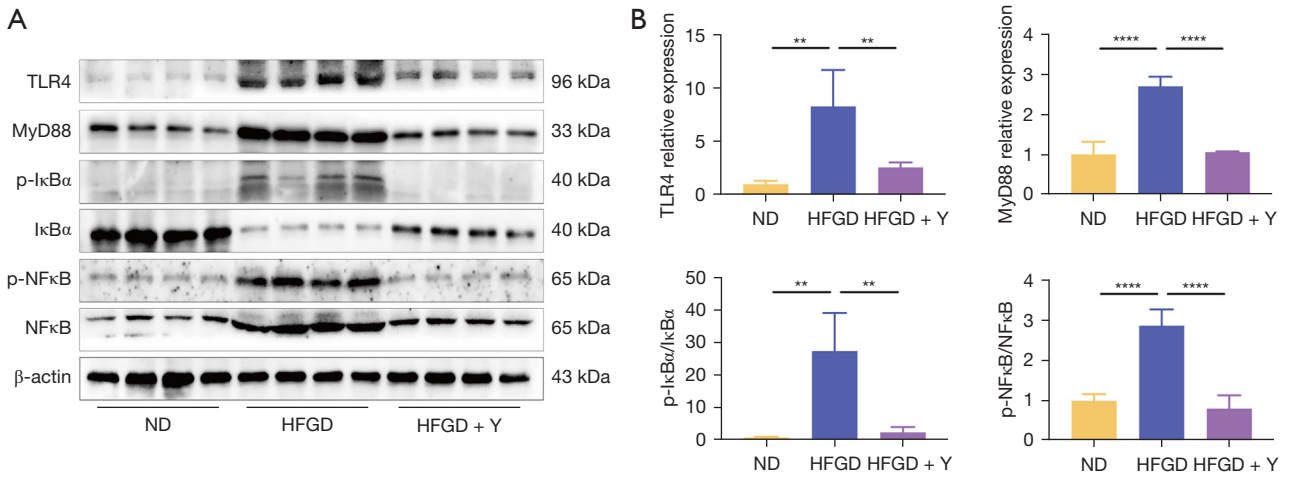

Figure 8 YZH attenuated NASH by inhibiting the hepatic TLR4, MyD88, NFκB pathway. (A) The expressions of TLR4, MyD88, IκBα, p-IκBα, NFκB and p-NFκB in the liver tissues of the 3 groups of mice were detected by Western Blot; (B) protein levels of TLR4, MyD88, IκBα, p-IκBα, NFκB and p-NFκB in 3 groups were calculated. Data were shown as mean ± SD. **P<0.01; ****P<0.0001. YZH, yinzhihuang; NASH, non-alcoholic steatohepatitis; TLR4, toll-like receptor 4; MyD88, myeloid differentiation primary response 88; NFκB, nuclear factor kappa B; IκBα, inhibitor of NFκB alpha.

a central role in the gut-liver axis through numerous metabolites (21). However, the precise association between gut microbiota and NASH presently remains unclear (45). Except for the perturbation of the intestinal microbiota occurring in patients with NASH (46), the 16S rRNA sequence data showed microbiota dysbiosis in NAFLD and NASH mouse models (47-49). The current study showed that YZH modulated the composition of gut microbiota rather than increasing the variety of intestinal microbiota. In addition, studies also reported that gut microbiota in obese humans and animals was associated with increased levels of *Firmicutes-to-Bacteroidetes* ratio (47,50,51), and effective treatment that reversed the ratio reduced obesity and hepatic steatosis (47,52). Findings of the current study showed that YZH treatment decreased the *Firmicutes-to-Bacteroidetes* ratio. Further analysis at the genus level revealed that YZH decreased the levels of *Mucispirillum*, *Helicobacter*, and *Desulfovibrionaceae*, which were increased in HFGD group. Moreover, previous studies showed that *Mucispirillum* was a genus associated with the early disruption of gut mucus layer (53) and that increased abundance of *Mucispirillum* reflected severe inflammatory response (54). *Helicobacter* is known to colonize in the intestinal mucosa (55). In addition, previous studies reported that *Helicobacter* could induce endoplasmic reticulum stress in intestinal epithelial cells and promote inflammation (56). *Desulfovibrionaceae* has also been shown to mediate chronic inflammation (57). It was found that the abundance of *Desulfovibrionaceae* was increased in animal models of metabolic syndrome (58) and NASH (59). Notably, it was found that *Desulfovibrionaceae* disrupted gut barrier because it reduced sulfate to H_2S (60). Therefore, the results of the current study showed that changing the composition of intestinal flora might be one of the mechanisms of YZH in NASH treatment.

Enterogenous inflammation is associated with gut barrier dysfunction (61), which is reflected in the imbalance of gut microbiota and increased intestinal permeability (62). In the present study, HFGD feeding led to increased intestinal permeability, characterized by edema and shortened intestinal microvilli, mitochondrial injury, and reduced expression of tight junction proteins (including, ZO-1, occludin, and claudin-1), which were recovered through treatment with YZH. Similarly, it was evident that YZH reduced the levels of serum LPS, TNF-α, and IL-6, while increased IL-10 in mice with NASH (*Figure 6*). It was reported that LPS is present in the cell walls of gram-negative bacteria and studies also showed that chronic inflammation and metabolic syndrome were associated with dysbiosis of the gut microbiota and elevated levels of serum LPS (50). Meanwhile, previous studies demonstrated that imbalance in the pro- and anti-inflammatory cytokines also played a crucial role in NASH (63). The association between pro- or anti-inflammatory cytokines and the progression or remission of NASH has not yet been reported (64). In

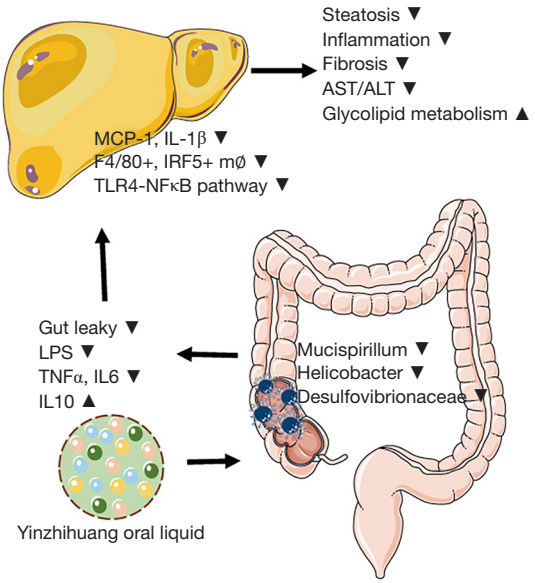

Figure 9 Graphic abstract. Yinzhihuang oral liquid effectively alleviated steatosis, inflammation, and fibrosis, reduced serum aspartate transaminase and alanine transaminase, and improved glycolipid metabolism of NASH mouse. Meanwhile, YZH treatment significantly decreased the abundance of harmful bacteria, such as *Mucispirillum*, *Helicobacter*, and *Desulfovibrionaceae*. Mechanistically, YZH reduced gut leaky, decreased serum LPS, IL-6, and TNF-α levels, and increased IL10 in serum. In the liver, YZH decreased MCP-1, IL-1β and alleviated macrophage infiltration, especially pro-inflammatory macrophages. Moreover, YZH inhibited the canonical TLR4, MyD88, NFκB signaling pathway. NASH, non-alcoholic steatohepatitis; YZH, yinzhihuang; LPS, lipopolysaccharide; IL-6, interleukin-6; TNF-α, tumor necrosis factor alpha; MCP-1, monocyte chemoattractant protein 1; IL-1β, interleukin-1 beta; TLR4, toll-like receptor 4; MyD88, myeloid differentiation primary response 88; NFκB, nuclear factor kappa B.

addition to the circulating inflammatory factors, YZH was also shown to reduce the infiltration of macrophages in the liver, especially the M1 pro-inflammatory macrophages, and the expression of MCP-1 and IL-1β in the liver. Previous study suggested pro-inflammatory sets of macrophages mediated the progression of NASH as well (65).

It was demonstrated that activation of the endotoxin, TLR4, NFκB pathway mediated gut dysbiosis and low-grade liver inflammation (66). Endotoxin/TLR4 was significantly upregulated in patients with NASH, as compared with those suffering from NAFLD and it was evident that the activation of TLR4 played an important role in the progression of NASH (67). Further, NFκB regulated liver injury and hepatic inflammation in NASH, suggesting that NFκB activation promoted NASH progression (68). It was shown that hepatic TLR4 expression was markedly elevated in HFGD group whereas YZH inhibited the expression of TLR4 and the activation of the downstream MyD88 and NFκB. This evidence in the current study demonstrated that YZH may alleviate liver injury in mice with NASH by restoring dysbiosis of the gut-liver axis (*Figure 9*).

Conclusions

In conclusion, the present study demonstrated that YZH could protect against NASH in HFGD mice. Further, it was evident that YZH exerted its effect through modulation of the gut microbiota, enhancement of intestinal barrier, reduction of endotoxins, and decreasing the infiltration of pro-inflammatory macrophages in the liver as well as inhibition of the TLR4, MyD88, NFκB pathway. Therefore, the multi-target characteristics of YZH provided a novel strategy for the prevention of NASH development and progression.

Acknowledgments

Funding: This work was supported by the National Natural Science Foundation of China (Nos. 81500460 and 82000575).

Footnote

Reporting Checklist: The authors have completed the ARRIVE reporting checklist. Available at https://atm.amegroups.com/article/view/10.21037/atm-21-4809/rc

Peer Review File: Available at https://atm.amegroups.com/article/view/10.21037/atm-21-4809/prf

Data Sharing Statement: Available at https://atm.amegroups.com/article/view/10.21037/atm-21-4809/dss

Conflicts of Interest: All authors have completed the ICMJE uniform disclosure form (available at https://atm.amegroups.com/article/view/10.21037/atm-21-4809/coif). The authors have no conflicts of interest to declare.

Ethical Statement: The authors are accountable for all

aspects of the work in ensuring that questions related to the accuracy or integrity of any part of the work are appropriately investigated and resolved. Experiments were performed under a project license (No. 2018-67) granted by the Ethics Review Committee of Zhongshan Hospital Fudan University. All animals were used and cared according to the criteria of the Chinese Animal Protection Act and the National Research Council.

References

1. Sheka AC, Adeyi O, Thompson J, et al. Nonalcoholic Steatohepatitis: A Review. JAMA 2020;323:1175-83.
2. Matteoni CA, Younossi ZM, Gramlich T, et al. Nonalcoholic fatty liver disease: a spectrum of clinical and pathological severity. Gastroenterology 1999;116:1413-9.
3. Csak T, Ganz M, Pespisa J, et al. Fatty acid and endotoxin activate inflammasomes in mouse hepatocytes that release danger signals to stimulate immune cells. Hepatology 2011;54:133-44.
4. Borrelli A, Bonelli P, Tuccillo FM, et al. Role of gut microbiota and oxidative stress in the progression of non-alcoholic fatty liver disease to hepatocarcinoma: Current and innovative therapeutic approaches. Redox Biol 2018;15:467-79.
5. de Faria Ghetti F, Oliveira DG, de Oliveira JM, et al. Influence of gut microbiota on the development and progression of nonalcoholic steatohepatitis. Eur J Nutr 2018;57:861-76.
6. Fukui H. Gut-liver axis in liver cirrhosis: How to manage leaky gut and endotoxemia. World J Hepatol 2015;7:425-42.
7. Mouries J, Brescia P, Silvestri A, et al. Microbiota-driven gut vascular barrier disruption is a prerequisite for non-alcoholic steatohepatitis development. J Hepatol 2019;71:1216-28.
8. Lee MM, Kim HG, Lee SB, et al. CGplus, a standardized herbal composition ameliorates non-alcoholic steatohepatitis in a tunicamycin-induced mouse model. Phytomedicine 2018;41:24-32.
9. Duan X, Meng Q, Wang C, et al. Calycosin attenuates triglyceride accumulation and hepatic fibrosis in murine model of non-alcoholic steatohepatitis via activating farnesoid X receptor. Phytomedicine 2017;25:83-92.
10. Xu G, Fu S, Zhan X, et al. Echinatin effectively protects against NLRP3 inflammasome-driven diseases by targeting HSP90. JCI Insight 2021;6:134601.
11. Xiao J, Wang F, Liong EC, et al. Lycium barbarum polysaccharides improve hepatic injury through NFkappa-B and NLRP3/6 pathways in a methionine choline deficient diet steatohepatitis mouse model. Int J Biol Macromol 2018;120:1480-9.
12. Zeng J, Wang SJ, Li YM, et al. Yinzhihuang oral liquid in the treatment of neonatal jaundice: a meta-analysis. Pharm Biol 2017;55:554-9.
13. Elferink RO. Yin Zhi Huang and other plant-derived preparations: where herbal and molecular medicine meet. J Hepatol 2004;41:691-3.
14. Sun W, Liu P, Wang T, et al. Baicalein reduces hepatic fat accumulation by activating AMPK in oleic acid-induced HepG2 cells and high-fat diet-induced non-insulin-resistant mice. Food Funct 2020;11:711-21.
15. Zhu X, Yao P, Liu J, et al. Baicalein attenuates impairment of hepatic lysosomal acidification induced by high fat diet via maintaining V-ATPase assembly. Food Chem Toxicol 2020;136:110990.
16. Hui Y, Wang X, Yu Z, et al. Scoparone as a therapeutic drug in liver diseases: Pharmacology, pharmacokinetics and molecular mechanisms of action. Pharmacol Res 2020;160:105170.
17. Liu B, Deng X, Jiang Q, et al. Scoparone improves hepatic inflammation and autophagy in mice with nonalcoholic steatohepatitis by regulating the ROS/P38/Nrf2 axis and PI3K/AKT/mTOR pathway in macrophages. Biomed Pharmacother 2020;125:109895.
18. Alqarni I, Bassiouni YA, Badr AM, et al. Telmisartan and/or chlorogenic acid attenuates fructose-induced non-alcoholic fatty liver disease in rats: Implications of cross-talk between angiotensin, the sphingosine kinase/sphingoine-1-phosphate pathway, and TLR4 receptors. Biochem Pharmacol 2019;164:252-62.
19. Yao Q, Li S, Cheng X, et al. Yin Zhi Huang, a traditional Chinese herbal formula, ameliorates diet-induced obesity and hepatic steatosis by activating the AMPK/SREBP-1 and the AMPK/ACC/CPT1A pathways. Ann Transl Med 2020;8:231.

20. Xin X, Jin Y, Wang X, et al. A Combination of Geniposide and Chlorogenic Acid Combination Ameliorates Nonalcoholic Steatohepatitis in Mice by Inhibiting Kupffer Cell Activation. Biomed Res Int 2021;2021:6615881.
21. Chu H, Duan Y, Yang L, et al. Small metabolites, possible big changes: a microbiota-centered view of non-alcoholic fatty liver disease. Gut 2019;68:359-70.
22. Liu XJ, Duan NN, Liu C, et al. Characterization of a murine nonalcoholic steatohepatitis model induced by high fat high calorie diet plus fructose and glucose in drinking water. Lab Invest 2018;98:1184-99.
23. Adkins Y, Schie IW, Fedor D, et al. A novel mouse model of nonalcoholic steatohepatitis with significant insulin resistance. Lab Invest 2013;93:1313-22.
24. Balog S, Li Y, Ogawa T, et al. Development of Capsular Fibrosis Beneath the Liver Surface in Humans and Mice. Hepatology 2020;71:291-305.
25. Li C, Zhou W, Li M, et al. Salvia-Nelumbinis naturalis extract protects mice against MCD diet-induced steatohepatitis via activation of colonic FXR-FGF15 pathway. Biomed Pharmacother 2021;139:111587.
26. Lan T, Yu Y, Zhang J, et al. Cordycepin Ameliorates Nonalcoholic Steatohepatitis via Activation of AMP-Activated Protein Kinase Signaling Pathway. Hepatology. 2021;74:686-703.
27. Wang Y, Tai YL, Zhao D, et al. Berberine Prevents Disease Progression of Nonalcoholic Steatohepatitis through Modulating Multiple Pathways. Cells 2021;10:210.
28. Hu Q, Zhang W, Wu Z, et al. Baicalin and the liver-gut system: Pharmacological bases explaining its therapeutic effects. Pharmacol Res 2021;165:105444.
29. Zeng J, Liu XL, Xin FZ, et al. Effects and therapeutic mechanism of Yinzhihuang on steatohepatitis in rats induced by a high-fat, high-cholesterol diet. J Dig Dis 2020;21:179-88.
30. Tsuchida T, Lee YA, Fujiwara N, et al. A simple diet- and chemical-induced murine NASH model with rapid progression of steatohepatitis, fibrosis and liver cancer. J Hepatol 2018;69:385-95.
31. Hong W, Li S, Cai Y, et al. The Target MicroRNAs and Potential Underlying Mechanisms of Yiqi-Bushen-Tiaozhi Recipe against-Non-Alcoholic Steatohepatitis. Front Pharmacol 2020;11:529553.
32. Luo Y, Burrington CM, Graff EC, et al. Metabolic phenotype and adipose and liver features in a high-fat Western diet-induced mouse model of obesity-linked NAFLD. Am J Physiol Endocrinol Metab 2016;310:E418-39.
33. Hirsova P, Ibrahim SH, Krishnan A, et al. Lipid-Induced Signaling Causes Release of Inflammatory Extracellular Vesicles From Hepatocytes. Gastroenterology 2016;150:956-67.
34. Ishimoto T, Lanaspa MA, Rivard CJ, et al. High-fat and high-sucrose (western) diet induces steatohepatitis that is dependent on fructokinase. Hepatology 2013;58:1632-43.
35. Rahman K, Desai C, Iyer SS, et al. Loss of Junctional Adhesion Molecule A Promotes Severe Steatohepatitis in Mice on a Diet High in Saturated Fat, Fructose, and Cholesterol. Gastroenterology 2016;151:733-746.e12.
36. Farrell G, Schattenberg JM, Leclercq I, et al. Mouse Models of Nonalcoholic Steatohepatitis: Toward Optimization of Their Relevance to Human Nonalcoholic Steatohepatitis. Hepatology 2019;69:2241-57.
37. Xu B, Li YL, Xu M, et al. Geniposide ameliorates TNBS-induced experimental colitis in rats via reducing inflammatory cytokine release and restoring impaired intestinal barrier function. Acta Pharmacol Sin 2017;38:688-98.
38. Zhang C, Wang N, Tan HY, et al. Direct inhibition of the TLR4/MyD88 pathway by geniposide suppresses HIF-1α-independent VEGF expression and angiogenesis in hepatocellular carcinoma. Br J Pharmacol 2020;177:3240-57.
39. Liu B, Deng X, Jiang Q, et al. Scoparone alleviates inflammation, apoptosis and fibrosis of non-alcoholic steatohepatitis by suppressing the TLR4/NF-κB signaling pathway in mice. Int Immunopharmacol 2019;75:105797.
40. Patwardhan RS, Sharma D, Thoh M, et al. Baicalein exhibits anti-inflammatory effects via inhibition of NF-κB transactivation. Biochem Pharmacol 2016;108:75-89.
41. Naveed M, Hejazi V, Abbas M, et al. Chlorogenic acid (CGA): A pharmacological review and call for further research. Biomed Pharmacother 2018;97:67-74.
42. Peng JH, Leng J, Tian HJ, et al. Geniposide and Chlorogenic Acid Combination Ameliorates Non-alcoholic Steatohepatitis Involving the Protection on the Gut Barrier Function in Mouse Induced by High-Fat Diet. Front Pharmacol 2018;9:1399.
43. Sampson TR, Mazmanian SK. Control of brain development, function, and behavior by the microbiome. Cell Host Microbe 2015;17:565-76.
44. Schnabl B, Brenner DA. Interactions between the intestinal microbiome and liver diseases. Gastroenterology 2014;146:1513-24.
45. Zhou D, Fan JG. Microbial metabolites in non-alcoholic fatty liver disease. World J Gastroenterol 2019;25:2019-28.
46. Wang Y, Wu Y, Wang B, et al. Bacillus amyloliquefaciens

SC06 Protects Mice Against High-Fat Diet-Induced Obesity and Liver Injury via Regulating Host Metabolism and Gut Microbiota. Front Microbiol 2019;10:1161.
47. Chang CJ, Lin CS, Lu CC, et al. Ganoderma lucidum reduces obesity in mice by modulating the composition of the gut microbiota. Nat Commun 2015;6:7489.
48. Xie X, Zhang L, Yuan S, et al. Val-Val-Tyr-Pro protects against non-alcoholic steatohepatitis in mice by modulating the gut microbiota and gut-liver axis activation. J Cell Mol Med 2021;25:1439-55.
49. Hua X, Sun DY, Zhang WJ, et al. P7C3-A20 alleviates fatty liver by shaping gut microbiota and inducing FGF21/FGF1, via the AMP-activated protein kinase/CREB regulated transcription coactivator 2 pathway. Br J Pharmacol 2021;178:2111-30.
50. Cani PD, Bibiloni R, Knauf C, et al. Changes in gut microbiota control metabolic endotoxemia-induced inflammation in high-fat diet-induced obesity and diabetes in mice. Diabetes 2008;57:1470-81.
51. Nuli R, Cai J, Kadeer A, et al. Integrative Analysis Toward Different Glucose Tolerance-Related Gut Microbiota and Diet. Front Endocrinol (Lausanne) 2019;10:295.
52. Liu L, Liu Z, Li H, et al. Naturally Occurring TPE-CA Maintains Gut Microbiota and Bile Acids Homeostasis via FXR Signaling Modulation of the Liver-Gut Axis. Front Pharmacol 2020;11:12.
53. Sun J, Qi C, Zhu H, et al. IgA-Targeted Lactobacillus jensenii Modulated Gut Barrier and Microbiota in High-Fat Diet-Fed Mice. Front Microbiol 2019;10:1179.
54. O'Connor KM, Lucking EF, Golubeva AV, et al. Manipulation of gut microbiota blunts the ventilatory response to hypercapnia in adult rats. EBioMedicine 2019;44:618-38.
55. Rhoades N, Barr T, Hendrickson S, et al. Maturation of the infant rhesus macaque gut microbiome and its role in the development of diarrheal disease. Genome Biol 2019;20:173.
56. Powell N, Pantazi E, Pavlidis P, et al. Interleukin-22 orchestrates a pathological endoplasmic reticulum stress response transcriptional programme in colonic epithelial cells. Gut 2020;69:578-90.
57. Vujkovic-Cvijin I, Sortino O, Verheij E, et al. HIV-associated gut dysbiosis is independent of sexual practice and correlates with noncommunicable diseases. Nat Commun 2020;11:2448.
58. Yang C, Qu Y, Fujita Y, et al. Possible role of the gut microbiota-brain axis in the antidepressant effects of (R)-ketamine in a social defeat stress model. Transl Psychiatry 2017;7:1294.
59. Zhang X, Coker OO, Chu ES, et al. Dietary cholesterol drives fatty liver-associated liver cancer by modulating gut microbiota and metabolites. Gut 2021;70:761-74.
60. Everard A, Lazarevic V, Derrien M, et al. Responses of gut microbiota and glucose and lipid metabolism to prebiotics in genetic obese and diet-induced leptin-resistant mice. Diabetes 2011;60:2775-86.
61. Strati F, Cavalieri D, Albanese D, et al. Altered gut microbiota in Rett syndrome. Microbiome 2016;4:41.
62. Noval Rivas M, Wakita D, Franklin MK, et al. Intestinal Permeability and IgA Provoke Immune Vasculitis Linked to Cardiovascular Inflammation. Immunity 2019;51:508-521.e6.
63. Schuppan D, Surabattula R, Wang XY. Determinants of fibrosis progression and regression in NASH. J Hepatol 2018;68:238-50.
64. Xiao L, Liang S, Ge L, et al. Si-Wei-Qing-Gan-Tang Improves Non-Alcoholic Steatohepatitis by Modulating the Nuclear Factor-κB Signal Pathway and Autophagy in Methionine and Choline Deficient Diet-Fed Rats. Front Pharmacol 2020;11:530.
65. de Oliveira S, Houseright RA, Graves AL, et al. Metformin modulates innate immune-mediated inflammation and early progression of NAFLD-associated hepatocellular carcinoma in zebrafish. J Hepatol 2019;70:710-21.
66. Porras D, Nistal E, Martínez-Flórez S, et al. Protective effect of quercetin on high-fat diet-induced non-alcoholic fatty liver disease in mice is mediated by modulating intestinal microbiota imbalance and related gut-liver axis activation. Free Radic Biol Med 2017;102:188-202.
67. Sharifnia T, Antoun J, Verriere TG, et al. Hepatic TLR4 signaling in obese NAFLD. Am J Physiol Gastrointest Liver Physiol 2015;309:G270-8.
68. Li R, Li J, Huang Y, et al. Polydatin attenuates diet-induced nonalcoholic steatohepatitis and fibrosis in mice. Int J Biol Sci 2018;14:1411-25.

Cite this article as: Li S, Chen F, Zou Y, Ning L, Zhang G, Zhang S, Yao Q. Yinzhihuang oral liquid protects against non-alcoholic steatohepatitis via modulation of the gut-liver axis in mice. Ann Transl Med 2022;10(11):631. doi: 10.21037/atm-21-4809

Supplementary

Table S1 Food intake of mice in each group

Time	Group ND (g)	Group HFGD (g)	Group HFGD + Y (g)
Week 1	5.05	5.14	5.69
Week 2	4.99	4.29	4.59
Week 3	4.93	5.14	4.74
Week 4	5.13	5.21	5.37
Week 5	5.15	5.29	5.62
Week 6	4.67	5.17	4.47
Week 7	4.84	4.44	5.55
Week 8	5.01	5.08	4.37
Week 9	5.15	5.43	5.63
Week 10	4.77	4.62	4.98
Week 11	4.95	5.11	5.09
Week 12	5.01	5.03	5.45
Week 13	4.84	4.99	5.86
Week 14	5.04	4.82	4.68
Week 15	5.21	5.15	5.64
Week 16	5.12	5.09	5.43

https://dx.doi.org/10.21037/atm-21-4809

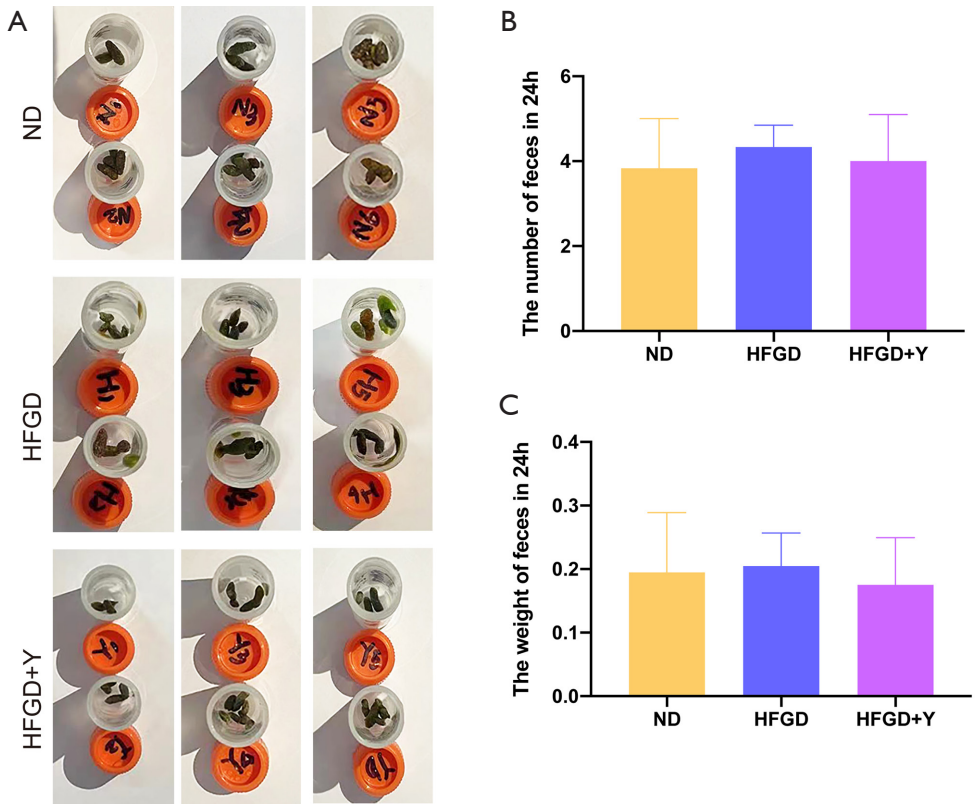

Figure S1 Shape and weight of feces, and number of pellets. (A) Shape of feces among groups; (B) number of pellets among groups in 24 h; (C) weight of feces among groups in 24 h. Data were shown as mean ± SD.

https://dx.doi.org/10.21037/atm-21-4809